Journal of Molecular Structure 1169 (2018) 59–67

Contents lists available at ScienceDirect

Journal of Molecular Structure

journal homepage: http://www.elsevier.com/locate/molstruc

Synthesis, crystal structure, Hirshfeld surface and DFT studies of ([Cu(3-ptp)$_2$(p-TS)$_2$]) from decomposition of tosylhydrazone

Murat Çınarlı [a], Çiğdem Yüksektepe Ataol [b, *], Murat Taş [c], Hümeyra Bati [d]

[a] Central Research and Application Laboratory, Ahi Evran University, 40100, Kirsehir, Turkey
[b] Department of Physics, Faculty of Science, Cankiri Karatekin University, Çankırı, Turkey
[c] Department of Science Education, Faculty of Education, Ondokuz Mayis University, 55139, Samsun, Turkey
[d] Department of Chemistry, Faculty of Science, Ondokuz Mayis University, 55139, Samsun, Turkey

ARTICLE INFO

Article history:
Received 27 February 2018
Accepted 14 May 2018
Available online 15 May 2018

Keywords:
Decomposition of tosylhydrazone
Single crystal structures
Metal complexes
DFT
Hirshfeld surface
DNA bases
NMR spectra

ABSTRACT

(3-ptp) and (p-TS) compounds are formed by decomposition of the tosylhydrazone ligand (LH). A mechanism for the decomposition of tosylhydrazone is proposed. The compounds formed by the decomposition coordinated to Cu(II) and its octahedral complex is formed. The single-crystal X-ray structure of the [Cu(3-ptp)$_2$(p-TS)$_2$] complex is reported by X-ray diffraction method and it is characterized by ^{1}H NMR technique. The [Cu(3-ptp)$_2$(p-TS)$_2$] complex is monoclinic crystal system and P 2$_1$ space group and contains two molecules in the unit cell (Z = 2, a = 8.09750(10) Å, b = 24.1689(4) Å, c = 8.9547(2) Å, β = 98.4070(10)°). In addition to the experimental X-ray analysis of the complex, the molecular structure of the complex was studied theoretically by using DFT of the computational chemistry methods. The complex is optimized with the B3LYP/6–31G method. In addition, molecular electrostatic potential mapping and the global reactivity parameters were obtained and the interactions between the molecule with DNA bases such as adenine, cytosine, guanine, and thymine was investigated by using the ECT (electrophilicity-based charge transfer) method and ΔN (charge transfer). Hirshfeld surface of Cu(II) complex was investigated and the interaction energies between the molecules participating in the C–H···O interactions in the complex structure were calculated by CE-HF energy model, and the energy values were found to be −212.01 and −73.07 kJ mol^{-1}.

1. Introduction

Since the report of Bamford and Stevens [1], a number of papers have been published [2,3] on the decomposition of tosylhydrazones.

Tosylhydrazones are important intermediates and have been used in organic synthesis for more than 60 years. The initial works in this include Bamford Stevens [1] and Shapiro [4] reactions both of which afforded alkenes. About 10 years ago, Aggarwal et al. utilized to sylhydrazone salts as diazo precursors in Wittigo lefination reactions [5], sulfurylide mediate depoxidation [6] and cyclo addition chemistry [7] under mild reaction conditions. In the presence of copper or palladium catalysts to sylhydrazones can react with terminal alkynes to form allenes [8], conjugate denynes [9] oral kynes [10]. This kind of transformation has been applied to the synthesis of phenanthrenes [11], benzofurans, and indoles [12].

Triazolopyridine structures are an important class of compounds form any pharmaceutical and functional materials. As an important class of triazolopyridines [1,2,3], triazolo [[,5-a]] pyridines have been studied by Jones et al. [13] and Abarca et al. [14] since the early 1980s. Traditionally, [1,2,3] triazolo [1,5-a] pyridines have been synthesized by the oxidative cyclization of 2-pyridyl ketone hydrazones by using at least a stoichiometric, if not an excess, amount of oxidants such as Pb(OAc)$_2$ [15], copper salts [16g,17], MnO$_2$ [3f,18], hyper valentiodine [19] Ag$_2$O [20] and Niperoxide [21].

In this work, we are investigated the single crystal structure of the copper complex, by X-ray diffraction analysis and its the theoretical calculations by Density Functional Theory (DFT) B3LYP/6–31G from computational chemistry methods. The complex structure is characterized by ^{1}H NMR spectra. By using DFT, the geometrical optimization of the complex was compared with X-ray results to the bond parameters, and its the electrophilic and

* Corresponding author.
E-mail addresses: yuksektepe.c@karatekin.edu.tr, yuksekc85@gmail.com (Ç.Y. Ataol).

https://doi.org/10.1016/j.molstruc.2018.05.047
0022-2860/

nucleophilic states were investigated by calculating the molecular electrostatic potential. Addition to these, the anionic, cationic and neutral states of the molecular structure and DNA bases are optimized and its energies are calculated by using DFT to observed the global reactivity parameters and also, the interactions between this compound and DNA bases are determined by using the ECT (electrophilicity-based charge transfer) method and the paratemeter ΔN (charge transfer).

2. Experimental

2.1. Physical measurements and theoretical methods

p-toluene sulfonyl hydrazide and di-2-pyridyl ketone were purchased from Sigma/Aldrich and used as received. ^{1}H NMR spectra was recorded on a Agilent Premium Compact 600 Spectrometer, using dmso-d^6 as a solvent. Starting geometries of the compound were taken from X-ray refinement data for computing procedure. The molecular structure of the compound in the ground state (*in vacuo*) was optimized by DFT methods to include correlation corrections with the 6–31G basis set. DFT forms hybrid functionals, including B3 [22], which defines the exchange functional as the linear combination of Hartree–Fock, local, and gradient-corrected exchange terms. The B3 hybrid functional was used in combination with the correlation functionals [23]. The molecular electrostatic potential of the molecular structure is calculated in order to determine the electrophilic and nucleophilic states of the molecule with B3LYP/6–31G. The Highest Occupied Molecular Orbital (HOMO) and the Lowest Unoccupied Molecular Orbital (LUMO) of the molecule were obtained by single point energy calculation in the Ground State (GS). The global reactivity parameters were evaluated using equations given in the Theoretical section. The anionic, cationic and neutral states of the molecular structure and DNA bases are optimized and its energies are calculated using DFT.

All the calculations were performed using Gaussian 09 program [24].

2.2. X-ray crystallography

X-ray diffraction data complex were obtained with a Bruker APEXII CCD diffractometer equipped with graphite-monochromated Mo-Kα radiation (λ = 0.71073 Å). The structure was solved by direct methods using SHELXS [25] implemented in the WinGX software system [26] and refined by the full-matrix least-squares procedure on F^2 using SHELXL [27]. All non-hydrogen atoms were easily found from the difference Fourier map and refined anisotropically. All hydrogen atoms were included using a riding model and refined isotropically with CH = 0.93 Å, CH_3 = 0.96 Å, $U_{iso}(H) = 1.5U_{eq}$ (1.2 for aromatic ring). Crystallographic data of the complex structure, details of the data collection and structure refinements are listed in Table 1.

2.3. Synthesis of the title compound

The compound was synthesized as shown in Scheme 1 by the following procedure. (N'-(dipyridin-2-ylmethylene)-4-methyl benzene sulfono hydrazone (LH) (0.142 g, 0.4 mmol) was dissolved in 20 mL MeOH-acetonitrile mixture. To this solution was added KOH (0.02 g, 0.4 mmol). To this solution was added dropwise $Cu(CH_3COO)_2 \cdot H_2O$ (0.049 g, 0.2 mmol) in 20 mL MeOH-acetonitrile mixture. The mixture was refluxed for 2–3 h and after cooling. The gren crystalline compound separated out and washed three times with ether. Crystal suitable for X-ray diffraction was collected.

It is believed that their action takes place in three steps:

Table 1
The crystal data of $[Cu(3\text{-ptp})_2(p\text{-TS})_2]$ complex.

Formula	$C_{36}H_{30}CuN_8O_6S_2$
Molecular weight	798.34
Temperature (K)	293
λ (Å)	0.71073, Mo-K_α
Crystal system	Monoclinic
Space group	P 2_1
a, b, c (Å)	8.09750(10), 24.1689(4), 8.9547(2)
α, β, γ (°)	90.00, 98.4070(10), 90.00
V(Å^3)	1733.67(5)
Z	2
$d_{calc.}$ (Mg.m^{-3})	1.529
Crystal size (mm)	0.450, 0.200, 0.150
θ range (°)	1.685–29.506
h, k, l range	h = −11 → 11, k = −33 → 33, l = −12 → 12
Reflections collected	19834
Independent reflections	9002
Observed reflections	7607
Goof (S)	1.036
R_1 (I > 2σ)	0.042
wR_2 (I > 2σ)	0.101
CCDC number	1578411

- Decomposition of to sylhydrazone (p-TS) (Bamford-Stevens)
- 3-(pyridin-2-yl)- [1–3]triazolo [1,5-a]pyridine(3-ptp) formed by the cyclization and oxidation of $SO_2$to SO_3.
- Octahedral complex occurred with Cu(II) (see Scheme 2).

3. Results and discussions

3.1. Determination of the crystal structure of the complex

The compounds (p-TS and 3-ptp) formed by the decomposition of the L^1H ligand are coordinated to the Cu^{2+} ion through pyridine-N, triazole N atoms and the O atom of the p-toluene sulfonic acid (see Fig. 1a). Each copper(II) ion shows a coordination number of six, binding with two oxygen atoms and four nitrogen atoms. In p-toluene sulfonate anion, S–O bond distance of anion shows characteristic values with S(1)–O(2) (1.441(4)Å), S(1)–O(3) (1.437(4) Å) and S(1)–O(1) (1.462(3)Å). S(1)–O(1) shows intermediate between single and double characters [28]. The O(1), O(4) atoms are from the sulfonate, and coordination bonds Cu–O(1) and Cu–O(4) are shorter than the normal Cu–O bond distances in the other complex [29]. The bond distances of N(6)–C(17) (1.337(5)Å) and N(2)–C(6) (1.340(5)Å) correspond more with a C–N single bond (1.48 Å) than a C=N double bond (1.30 Å) [30]. The local coordination of copper (II) is an almost perfect octahedral environment, the sum of angles being 360.00°.

In Fig. 1a, the crystal structure has been shown. The crystal data can be seen from Table 1. It can be seen that the bond parameters of the single crystal structure are given in Table 2. The bond parameters of this study were found to be quite consistent when compared to similar studies.

In the molecular structure, C–H···N and C–H···O intramolecular with C–H···O intermolecular hydrogen bonds are observed. Figs. 2 and 3 are shown the crystal packing of the single crystal structure with different intermolecular hydrogen bonds. Also, the hydrogen bond parameters are shown in Table 3. It can be seen from Figs. 2 and 3 that C4–H4···O1^{i}, C8–H8···O1^{i}, C15–H15···O4^{ii} and C19–H19···O4^{ii} with C21–H21···O3^{iii}, C10–H10···O6^{iv} intermolecular hydrogen bonds create a chain along the [100] direction of the unit cell. The layer formed by these chains continues along the direction *b* of the unit cell to stabilize the crystal structure (see Figs. 2 and 3).

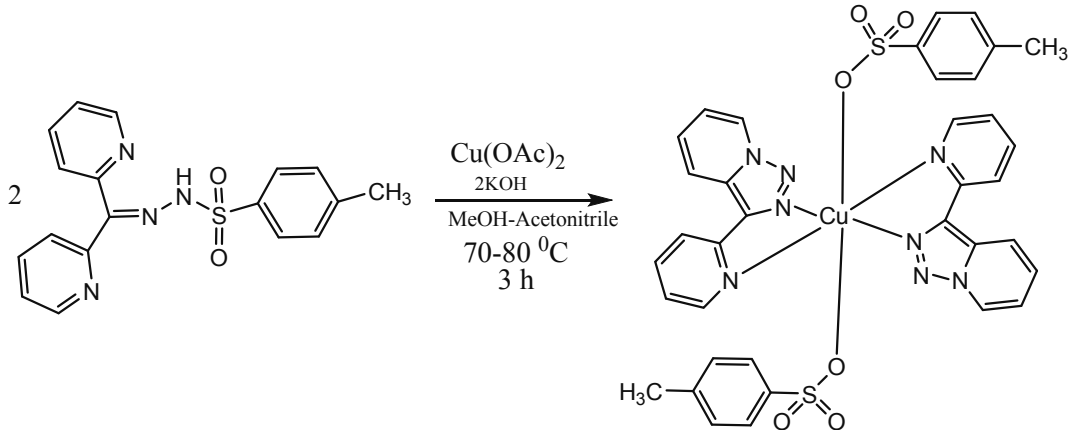

Scheme 1. Synthesis of title compound ([Cu(3-ptp)$_2$(p-TS)$_2$]).

3.2. ^{1}H NMR spectra of the [Cu(3-ptp)$_2$(p-TS)$_2$] complex

The NMR technique is used to detect the presence of particular nuclei in a compound for a given nuclear species. It is also an important tool for the identification of molecules and for the examination of their electronic structure [31]. The ^{1}H NMR spectrum of [Cu(3-ptp)$_2$(p-TS)$_2$] is not very well resolved. This may be due to partial oxidation of the metal centre in the solution to give a paramagnetic d^{9}copper(II) ion [32]. However, the sharp singlet at δ 2.26 is due to −CH$_3$ protons of p-toluene sulfonate moiety. In the aromatic regions, peaksat 7–7.3 ppm corresponds to p-toluene rings. The peaksat 7.4–7.8 ppm and at 8.6 ppm area ssigned to pyridine and [1,2,3] triazolo [1,5-a] pyridine rings, respectively. In the structure, it was observed C–H proton peaks in the p-toluene and [1,2,3] triazolo [1,5-a] pyridine rings shift to 5.8 ppm and 8.98 ppm respectively, because of the formation of intramolecular C–H···O and C–H···N hydrogen bonds [33] (see Fig. 4).

3.3. Hirshfeld surface of the crystal structure

The Hirshfeld surface [34,35] of a molecule in a crystal is constructed by partitioning space in the crystal into regions where the electron distribution of a sum of spherical atoms for the molecule (the promolecule) dominates the corresponding sum over the crystal (the procrystal). Following Hirshfeld [36], we define a molecular weight function $w(\mathbf{r})$:

$$w(r) = \frac{\rho_{promolecule}(r)}{\rho_{prpcrystal}(r)} \tag{1}$$

$$w(r) = \frac{\sum_{A \in molecule} \rho_A(r)}{\sum_{A \in crystal} \rho_A(r)} \tag{2}$$

$\rho_A(r)$, is a spherically-averaged atomic electron density centered on nucleus A, and the promolecule and procrystal are summed over the atoms belonging to the molecule and to the crystal, respectively. The Hirshfeld surface is then defined in a crystal as that region around a molecule where $w(\mathrm{r}) \geq 0.5$. That is the region where the promolecule contribution to the procrystal electron density exceeds that from all other molecules in the crystal. The simplest and most immediately useful property to map onto the surface is the distance from the surface to the nearest nucleus external to the surface, which we call d_e. This property provides an immediate picture of the nature of intermolecular contacts in the crystal.

In a similar fashion, we can define d_i, the distance from the surface to the nearest nucleus internal to the surface, which is valuable when used in conjunction with d_e. d_{norm} is a normalized contact distance. d_i is normalized by the van der Waals radius of the atom involved; d_e is similarly normalized, and the sum of these two quantities is the d_{norm} property [37]:

$$d_{norm} = \frac{d_i - r_i^{vdW}}{r_i^{vdW}} + \frac{d_e - r_e^{vdW}}{r_e^{vdW}} \tag{3}$$

where atoms make intermolecular contacts closer than the sum of their van der Waals radii, these contacts will be highlighted in red on the d_{norm} surface. The energy of interaction between molecules is commonly expressed in terms of four key components: electrostatic, polarization, dispersion, and exchange-repulsion:

$$E_{tot} = k_{ele}E_{ele} + k_{pol}E_{pol} + k_{dis}E_{dis} + k_{rep}E_{rep} \tag{4}$$

where k is the scale factor and E_{tot} is the total energy.

The intermolecular interactions of the title compound are quantified using Hirshfeld surface analysis. CrystalExplorer Software is used in the calculations [38]. The mapping of d_i, d_e, d_{norm}, shape index and curvedness of [Cu(3-ptp)$_2$(p-TS)$_2$] complex is shown in Fig. 5. These inter-contacts (C–H···O) are highlighted by conventional mapping of d_{norm} on molecular Hirshfeld surfaces as shown in Fig. 6 for [Cu(3-ptp)$_2$(p-TS)$_2$] complex and the energies of the interaction (E_{tot}) between the molecules are calculated by CE-HF energy model (see Table 4). The interaction energies between the molecules participating in the C–H···O interactions in the [Cu(3-ptp)$_2$(p-TS)$_2$] complex were calculated by CE-HF energy model, and the energy values for (x, y, z) and (−1+x, y, z), (x, y, z) and (1 + x, y, z), (x, y, z) and (x, y, −1+z) with (x, y, z) and (x, y, 1 + z) the symmetry coded molecules were found to be −212.01, −212.01, −73.07, and −73.07 kJ mol^{-1}, respectively. The calculation results show that although the molecules have different symmetries, the energy values for the two molecular structures are the same because the R distance between the molecular centers is the same.

The red spots on the surface indicate the intercontacts involved in the hydrogen bonds. Further, intercontacts are plotted with fingerprint plots Fig. 7: Figures show large surfaces for all intercontacts, H···H intercontacts, C···H, O···H, and N···H contacts plot reveals the information of intermolecular hydrogen bonds.

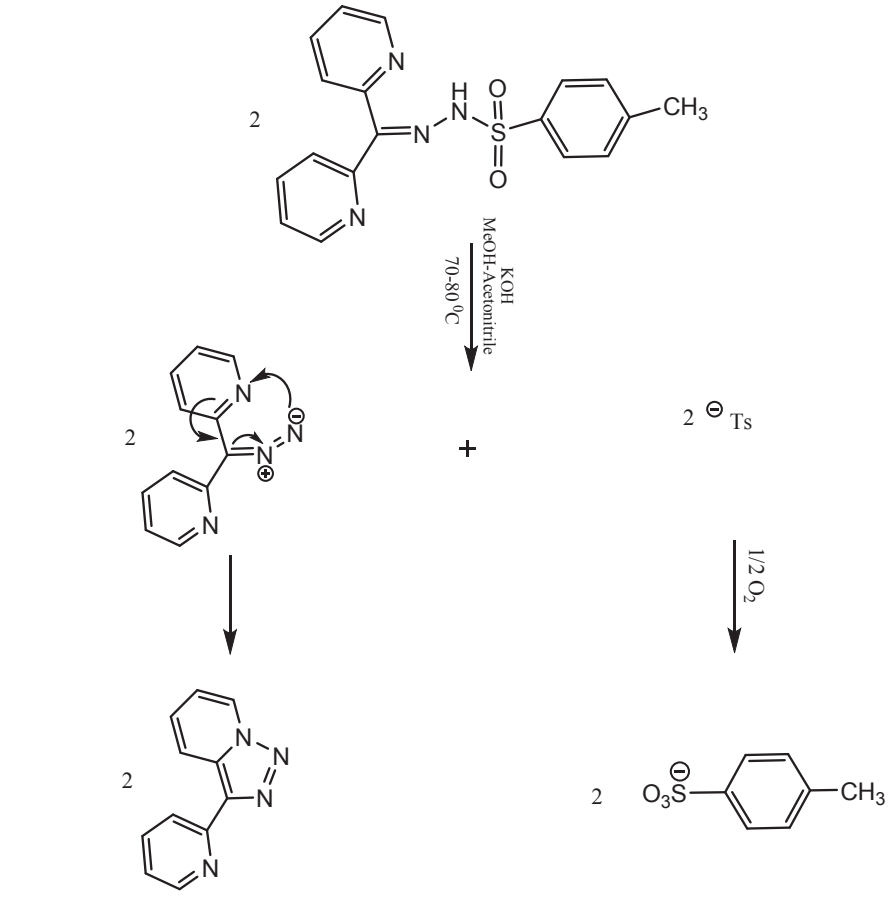

3-(pyridin-2-yl)-[1,2,3]triazolo[1,5-*a*]pyridine

Scheme 2. Propose mechanism of decomposition to sylhydrazone and synthesis of $[Cu(3\text{-}ptp)_2(p\text{-}TS)_2]$.

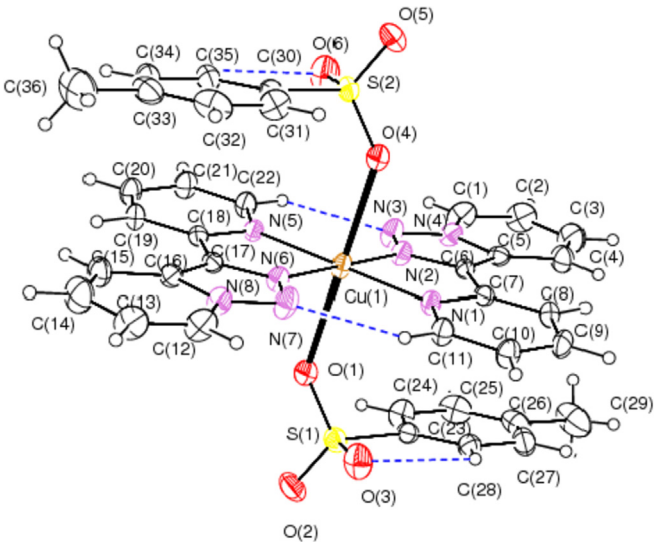

Fig. 1a. The crystal structure of $[Cu(3\text{-ptp})_2(p\text{-TS})_2]$.

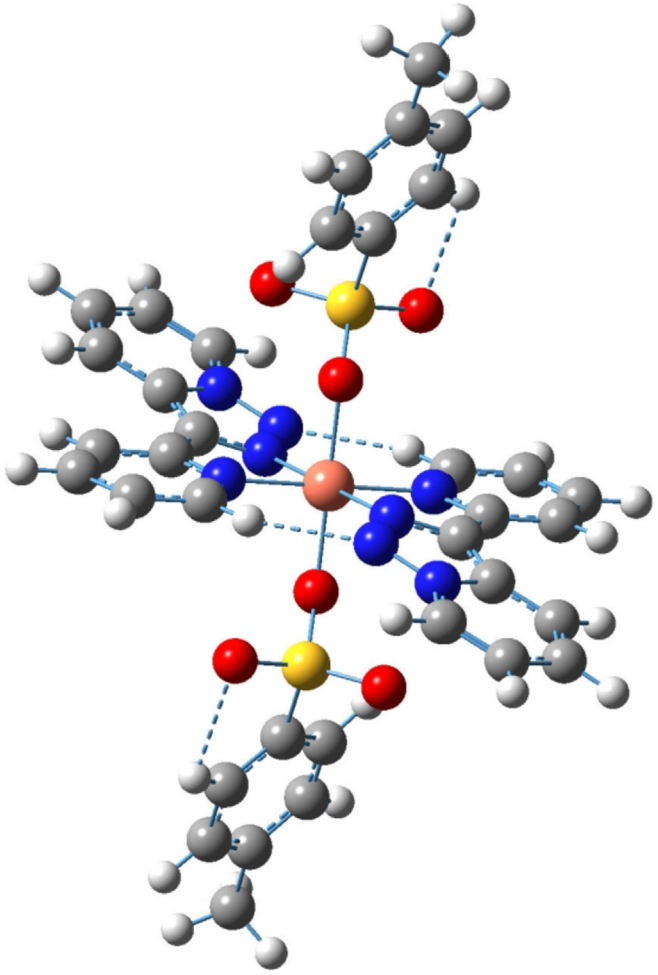

Fig. 1b. The molecular structure of $[Cu(3\text{-ptp})_2(p\text{-TS})_2]$ calculated by B3LYP/6-31G.

3.4. Theoretical studies using DFT method

3.4.1. Optimized structure

Fig. 1b shows the optimized structure of the single crystal. The optimized molecular geometry is calculated by using B3LYP/6−31G method. The bond parameters obtained from X-rays and the optimized molecular parameter by B3LYP/6−31G method are comparatively given in Table 2. Experimental results are the solid phase and theoretical calculations are the gaseous phase. In the solid state, intermolecular interactions connect molecules, resulting in differences of bond parameters between calculated and experimental values. It is well known that DFT optimized geometric parameters are usually good agreement with experimental values and more accurate than Hartree-Fock and semi-empirical methods, due to the inclusion of electron correlation. The root-mean-square error (RMSE) is used the measure of the differences between the calculated and observed values. This study, RMSE values are 0.1962Å for bond lengths and 2.2353° for bond angles by using B3LYP/6−31G method, respectively.

As can be seen in Table 2, the optimized bond lengths and bond angles are the good agreement to the experimental values.

3.4.2. Molecular electrostatic potential

Fig. 8 shows the electrostatic potential map of the molecule structure by using B3LYP/6−31G method. The molecular electrostatic potential surface MESP which is a 3D plot of electrostatic potential mapped onto the iso-electron density surface simultaneously displays molecular shape, size and electrostatic potential values. The molecular electrostatic potential map (MEP) shows that the red color (low potential region) is the electronically rich region (nucleophilic) and the blue color (high potential region) is the poor region of electrons (electrophilic). The oxygen atoms of the sulfanate have a higher electronegativity value (nucleophilic) would consequently have a higher electron density around them. Thus the spherical region that corresponds to oxygen atom would have a red portion of it. MESP surface shows that between molecules having different symmetries will be an intermolecular interaction. The molecular electrostatic potential map is shown in Fig. 8.

3.4.3. Global reactivity descriptors

The complex structure of Cu(II) with adenine, cytosine, guanine, and thymine of the DNA bases are optimized by using B3LYP/6−31G method in GS. And then, using the optimized structures, its the single point energies are calculated for its anion, cation and neutral states by B3LYP/6−31G method.

Chemical potential (μ) and molecular hardness (η) for the N-electron system with the total energy of E and external potential of V(r) are defined respectivelyas the first and second derivatives of energy with respect to N [39,40]:

$$\mu = \left[\frac{\partial E}{\partial N}\right]_{V(\vec{r})} = -\chi \tag{1}$$

and:

$$\eta = \frac{1}{2}\left[\frac{\partial^2 E}{\partial N^2}\right]_{V(\vec{r})} = \frac{1}{2}\left[\frac{\partial \mu}{\partial N}\right] \tag{2}$$

where χ(eV) in Eq. (1) is electronegativity. In numerical applications, μ and η are calculated through the use of difference approximation:

Table 2
Bond lengths and bond angles of $[Cu(3\text{-ptp})_2(p\text{-TS})_2]$ complex.

Bond lengths and bonds (Å, °)	Experimental	Theoretical		Experimental	Theoretical
Cu–N(6)	2.022(4)	2.348	S(2)–O(6)	1.440(4)	1.646
Cu–N(2)	2.024(4)	2.346	S(2)–O(4)	1.457(3)	1.699
Cu–N(5)	2.036(3)	2.029	N(4)–N(3)	1.350(5)	1.388
Cu–N(1)	2.040(3)	2.029	N(4)–C(5)	1.365(5)	1.395
Cu–O(4)	2.374(4)	2.013	N(8)–N(7)	1.357(5)	1.388
Cu–O(1)	2.376(4)	2.013	N(2)–N(3)	1.319(5)	1.327
S(1)–O(3)	1.439(4)	1.646	N(2)–C(6)	1.340(5)	1.366
S(1)–O(2)	1.441(4)	1.645	N(6)–N(7)	1.320(5)	1.327
S(1)–O(1)	1.462(3)	1.699	N(6)–C(17)	1.337(5)	1.366
S(2)–O(5)	1.437(4)	1.645	S(1)–C(23)	1.772(4)	1.865
RMSE			0.1962		
N(6)–Cu–N(2)	179.9(2)	179.9	N(2)–Cu–N(1)	80.4(13)	77.3
N(6)–Cu–N(5)	80.5(13)	77.3	N(5)–Cu–N(1)	179.8(17)	180.0
N(2)–Cu–N(5)	99.4(13)	102.7	N(6)–Cu–O(4)	90.6(14)	88.6
N(6)–Cu–N(1)	99.5(13)	102.7	N(6)–Cu–N(5)	80.5(13)	77.3
N(2)–Cu–N(1)	80.4(13)	77.3	O(6)–S(2)–O(4)	113.2(3)	113.8
N(5)–Cu–N(1)	179.8(17)	180.0	N(7)–N(8)–C(12)	123.8(4)	124.5
N(6)–Cu–O(4)	90.6(14)	88.6	S(1)–O(1)–Cu	133.3(2)	129.4
N(6)–Cu–O(1)	89.4(15)	91.4	S(2)–O(4)–Cu	133.2(2)	129.5
N(2)–Cu–O(1)	90.5(14)	88.7	N(3)–N(2)–C(6)	111.7(3)	111.9
N(2)–Cu–N(5)	99.4(13)	102.7	N(3)–N(2)–Cu	134.8(3)	137.5
N(6)–Cu–N(1)	99.5(13)	102.7	O(3)–S(1)–O(1)	112.5(3)	113.8
O(4)–Cu–O(1)	179.8(13)	180.0	O(2)–S(1)–O(1)	111.8(2)	111.0
O(3)–S(1)–O(2)	113.9(3)	115.2	O(5)–S(2)–O(6)	114.0(3)	115.2
O(5)–S(2)–O(4)	111.2(2)	111.0	N(6)–Cu–N(2)	179.9(2)	180.0
RMSE			2.2353		

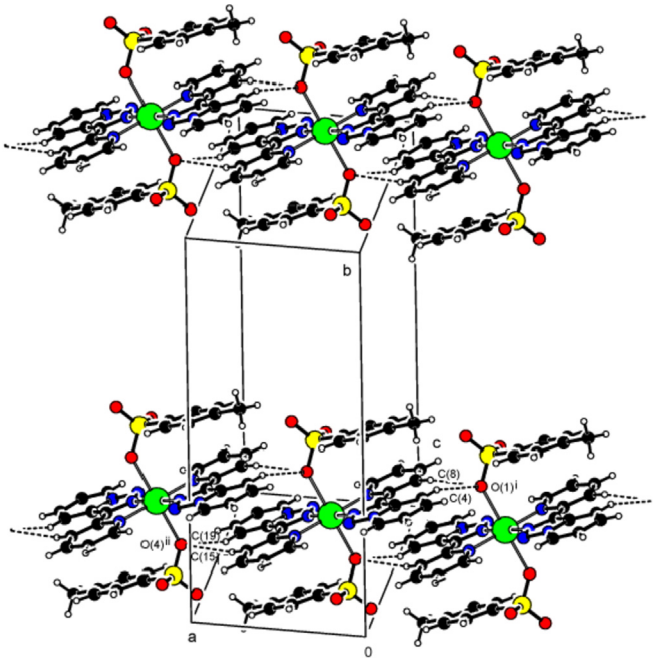

Fig. 2. Hydrogen bond interactions of the $[Cu(3\text{-ptp})_2(p\text{-TS})_2]$ complex. Symmetry codes: (i): −1+x, y, z (ii): 1 + x, y, z.

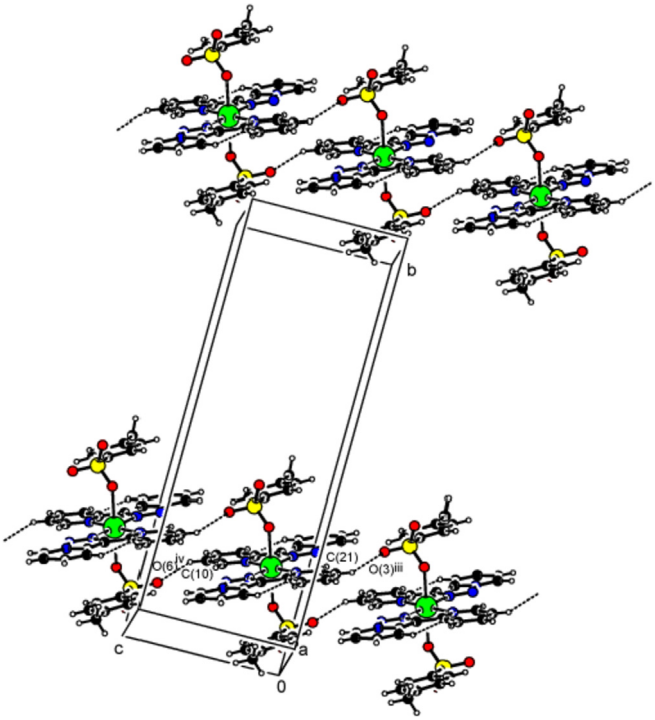

Fig. 3. Unit cell stacking of the $[Cu(3\text{-ptp})_2(p\text{-TS})_2]$ complex. Symmetry codes: (iii); x, y, −1+z (iv) x, y, 1 + z.

$$\mu = -\frac{1}{2}(IP + E_A) \tag{3}$$

$$\eta = \frac{1}{2}(IP - E_A) \tag{4}$$

Vertical Ionization Potential (IP) and Electron Affinity (E_A) can be obtained from the energy of neutral, anionic, and cationic species at the geometry of corresponding N electron neutral species, as follows:

$$IP = [E(N-1) - E(N)] \tag{5}$$

$$E_A = [E(N) - E(N+1)] \tag{6}$$

Electrophilicity index (ω) and global softness (S) are defined as follows:

Table 3
Hydrogen bond parameters of the molecular structure.

D–H···A	D–H(Å)	H···A(Å)	D···A (Å)	D–H···A (°)
C(22)–H(22)···N(3)	0.93	2.35	3.139(1)	143
C(11)–H(11)··· N(7)	0.93	2.34	3.134(1)	143
C(28)–H(28)··· O(3)	0.93	2.50	2.890(1)	106
C(35)–H(35)··· O(6)	0.93	2.50	2.888(1)	105
C(4)–H(4)··· O(1)^{i}	0.93	2.50	3.377(1)	158
C(8)–H(8)··· O(1)^{i}	0.93	2.51	3.373(1)	155
C(15)–H(15)··· O(4)^{ii}	0.93	2.49	3.368(1)	157
C(19)–H(19)··· O(4)^{ii}	0.93	2.52	3.378(1)	153
C(21)–H(21)··· O(3)^{iii}	0.93	2.446(4)	3.262(4)	146.37
C(10)–H(10)··· O(6)^{iv}	0.93	2.458(4)	3.687(4)	140.22

D = Donor, H= Hydrogen, A = Acceptor, Symmetry codes: (i): −1+x, y, z (ii): 1 + x, y, z (iii); x, y, −1+z (iv) x, y, 1 + z.

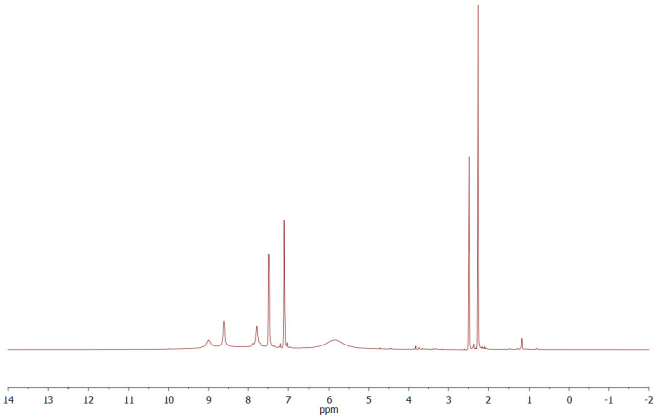

Fig. 4. ^{1}H NMR spectra of the [Cu(3-ptp)$_2$(p-TS)$_2$] complex.

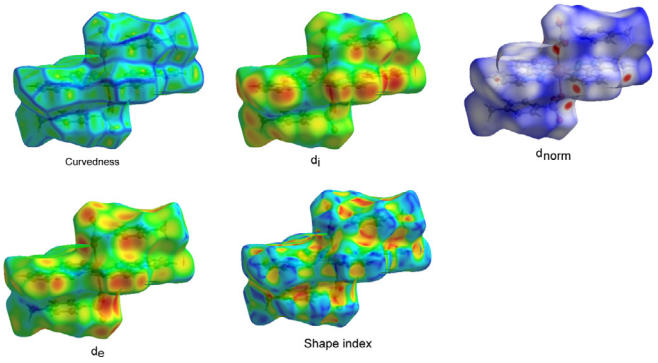

Fig. 5. Curvedness, d$_i$, d$_{norm}$, d$_e$, and shape index for [Cu(3-ptp)$_2$(p-TS)$_2$].

$$\omega = \frac{\mu^2}{2\eta} \tag{7}$$

$$S = \frac{1}{\eta} \tag{8}$$

According to Parr et al. [40], electrophilicity index (ω) is a global reactivity index similar to chemical hardness and chemical potential. This new reactivity index measures the stabilization in energy when the system reserves additional the electronic charge (ΔN). The direction of charge transfer is determined by the electronic chemical potential of the molecule because an electrophile is a chemical species capable of accepting electrons from the environment; its energy must decrease upon accepting the electronic

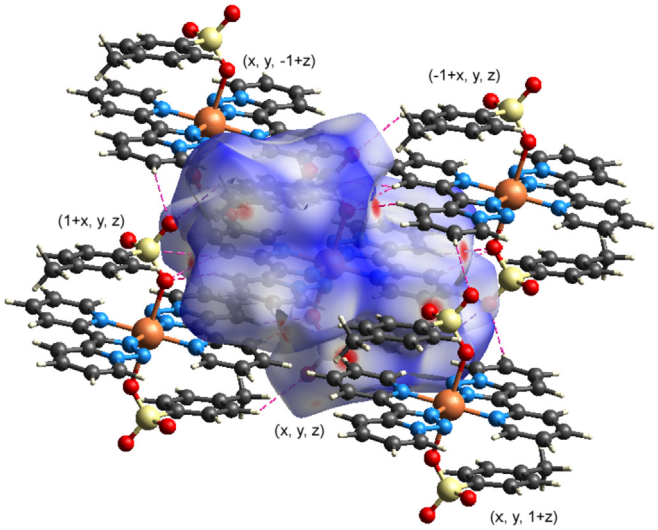

Fig. 6. d$_{norm}$ mapped on Hirshfeld surface for visualizing the intercontacts of [Cu(3-ptp)$_2$(p-TS)$_2$]. Dotted red lines represent hydrogen bonds (C(4)–H(4)··· O(1)^{i}, C(8)–H(8)··· O(1)^{i}, C(15)–H(15)··· O(4)^{ii}, C(19)–H(19)··· O(4)^{ii}, C(21)–H(21)··· O(3)^{iii} and C(10)–H(10)··· O(6)^{iv} symmetry codes: (i) −1+x, y, z, (ii) 1 + x, y, z, (iii) x, y, −1+z, and (iv) x, y, 1 + z.

charge. So its electronic chemical potential must be negative. χ, μ, η, S, and ω for the complex structure are listed in Table 5. In a reaction between two molecules, species can act as a nucleophile which has a lower value of electrophilicity index. The values of electrophilicity index listed in Table 5 show that the adenine, guanine, cytosine, and thymine from DNA basis are good nucleophiles so that they can attack the [Cu(3-ptp)$_2$(p-TS)$_2$]. Electrophilic Charge Transfer (ECT) [41] is explained as the difference between ΔN$_{max}$ values of interacting molecules. We consider two molecules A (the [Cu(3-ptp)$_2$(p-TS)$_2$]) and B (adenine, cytosine, guanine, and thymine) approach each other, where two cases exit: (i) ECT > 0, charge ow from B to A; and (ii) ECT < 0, charge ow from A to B. ECT is calculated by the following equation:

$$ECT = (\Delta N_{\max})_A - (\Delta N_{\max})_B \tag{9}$$

where $(\Delta N_{\max})_A = \mu_A/\eta_A$ and $(\Delta N_{\max})_B = \mu_B/\eta_B$.

ECT is calculated as −0.2802, −0.3738, −0.029, and −0.8856 for the adenine, cytosine, guanine, and thymine, respectively. These results show that electrons are transferred from the [Cu(3-ptp)$_2$(p-TS)$_2$] to the DNA bases. Therefore, the DNA bases treat as the electron acceptor and so the [Cu(3-ptp)$_2$(p-TS)$_2$] as the electron donor. So the DNA bases have electrophilic behavior while the [Cu(3-ptp)$_2$(p-TS)$_2$] has nucleophilic behavior.

3.4.4. HOMO and LUMO energies of the molecular structure

A large part of the theoretical chemistry related to reactivity is based on the concept of the Frontier Molecular Orbitals (FMO), especially the Lowest Unoccupied Molecular Orbital (LUMO) and the Highest Occupied Molecular Orbital (HOMO). The interaction between these orbitals often allows for a good description of the reactivity of reactions. The FMO theory says that attack of an electrophilic species will take place where there is more density of the HOMO, whereas attack of a nucleophilic species will take place in a region with the higher density of the LUMO. The frontier orbital energy gap helps characterize the chemical reactivity and kinetic stability of the molecule. A molecule with a small frontier orbital gap is more polarizable and is generally associated with a high chemical reactivity, low kinetic stability and is also termed as the

Table 4
The scaled total energies of the interactions between the molecules. R is the distance between molecular centroids (mean atomic position in Å. The scaled total energies are sum of the scaled four energy compenents in kJ mol^{-1}.

M	Symop	R	Electron Density	E_{ele}	E_{pol}	E_{dis}	E_{rep}	E_{tot}
1	−1+x, y, z	8.10	HF/3–21G	−108.83	−53.90	−111.81	62.53	−212.01
2	1 + x, y, z	8.10	HF/3–21G	−108.83	−53.90	−111.81	62.53	−212.01
3	x, y, −1+z	8.95	HF/3–21G	−16.81	−25.13	−55.14	24.01	−73.07
4	x, y, 1 + z	8.95	HF/3–21G	−16.81	−25.13	−55.14	24.01	−73.07

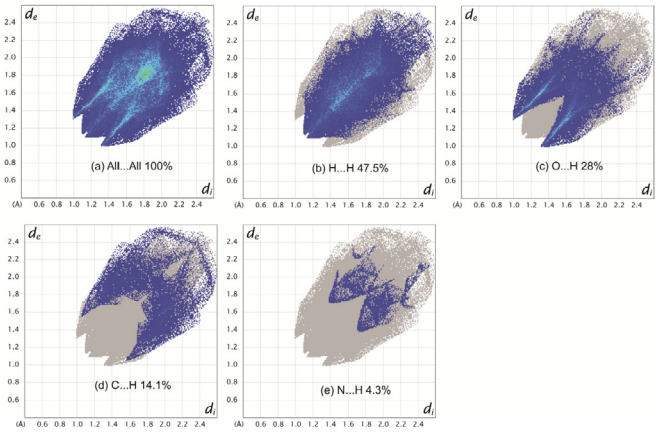

Fig. 7. The 2D-fingerprint plot of the Hirshfeld surface of $[Cu(3\text{-ptp})_2(p\text{-TS})_2]$.

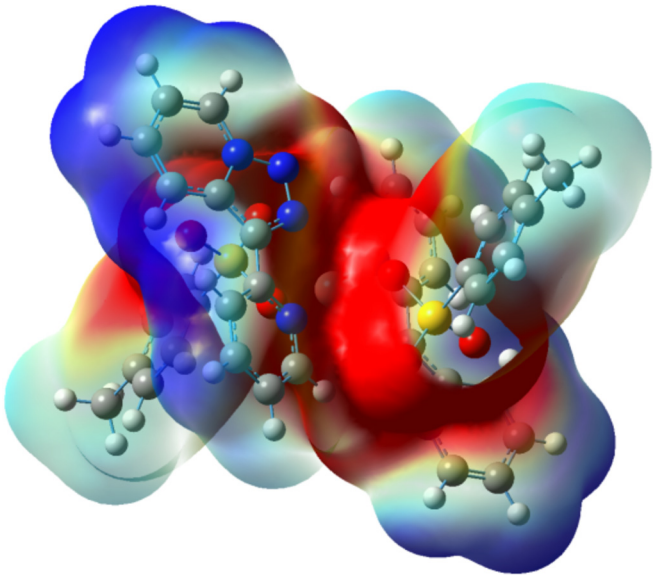

Fig. 8. The molecular electrostatic potantial map of the molecular structure.

soft molecule. The HOMO is the orbital that primarily acts as an electron donor and the LUMO is the orbital that largely acts as the electron acceptor. The highest occupied molecular (HOMO), the lowest unoccupied molecular orbital (LUMO) energies and HOMO and LUMO energy gap (E_{HOMO} - E_{LUMO}) are found at −8.1444, −1.6360 and −6.5084 eV by DFT/6–31G basis set in the gas phase. The 3D plots of the frontier orbitals HOMO and LUMO levels for $[Cu(3\text{-ptp})_2(p\text{-TS})_2]$ are shown in Fig. 9. Parr and co-workers have demonstrated that nearly the whole frontier molecular theory can be rationalized from the Density Functional Theory (DFT) [42].

4. Conclusion

This work includes the synthesis and characterization of the mononuclear $[Cu(3\text{-ptp})_2(p\text{-TS})_2]$ complex. The complex structure is investigated with X-ray diffraction analysis and DFT from computational chemistry methods. X-ray results are shown that the mononuclear complex structure crystallizes monoclinic crystal system and $P2_1$ space group. We can say that intermolecular C—H···O hydrogen bonds stabilize the crystal packing structure. Some of the peaks were observed to be shifted due to intramolecular hydrogen bonds from the ^1H NMR results. Hirsfeld surface analysis and intermolecular interaction energy calculation results show that molecules with symmetries (−1+x, y, z) and (1 + x, y, z) have the stronger interaction with the symmetric molecule (x, y, z) than other symmetric structures are showing. We can say that this could be because the distance R between the molecular centers is short. Besides of these, we can say that the optimized bond lengths and bond angles are the good agreement to the experimental values. The molecular electrostatic potential map is shown that the oxygen atoms in the molecule are nucleophilic and the regions where the carbon atoms are dense have a high potential region (electrophilic). The global reactivity parameters of the molecular structure and DNA bases such as adenine, cytosine, guanine, and thymine are calculated by DFT. The results show that electrons are transferred from the $[Cu(3\text{-ptp})_2(p\text{-TS})_2]$ to the DNA bases. Therefore, the DNA bases treat as the electron acceptor and so the $[Cu(3\text{-ptp})_2(p\text{-TS})_2]$ as the electron donor. So the DNA bases have electrophilic behavior while the $[Cu(3\text{-ptp})_2(p\text{-TS})_2]$ has nucleophilic behavior. Given the ECT values, it can be said that the molecule can interact more with thymine. It can be said from the

Table 5
The calculated χ, μ, η, S, ω, ΔN in eV at DFT/6-31G level in gas phase.

Compounds	IP (eV)	EA (eV)	χ (eV)	μ (eV)	η (eV)	S (eV^{-1})	ω (eV)	ΔN
$[Cu(3\text{-ptp})_2(p\text{-TS})_2]$	0.1932	−6.8138	−3.3103	3.3103	3.5035	0.2854	1.5639	0.4449
Adenine	1.3007	−8.1608	−3.4300	3.4300	4.7307	0.2114	1.2435	0.7251
Cytosine	0.8381	−8.4084	−3.7851	3.7851	4.6232	0.2163	1.3406	0.8187
Guanine	1.8830	−7.7390	−2.928	2.928	4.811	0.2079	0.8910	0.4739
Thymine	−1.3905	−9.8043	−5.5974	5.5974	4.2069	0.2377	3.7237	1.3305

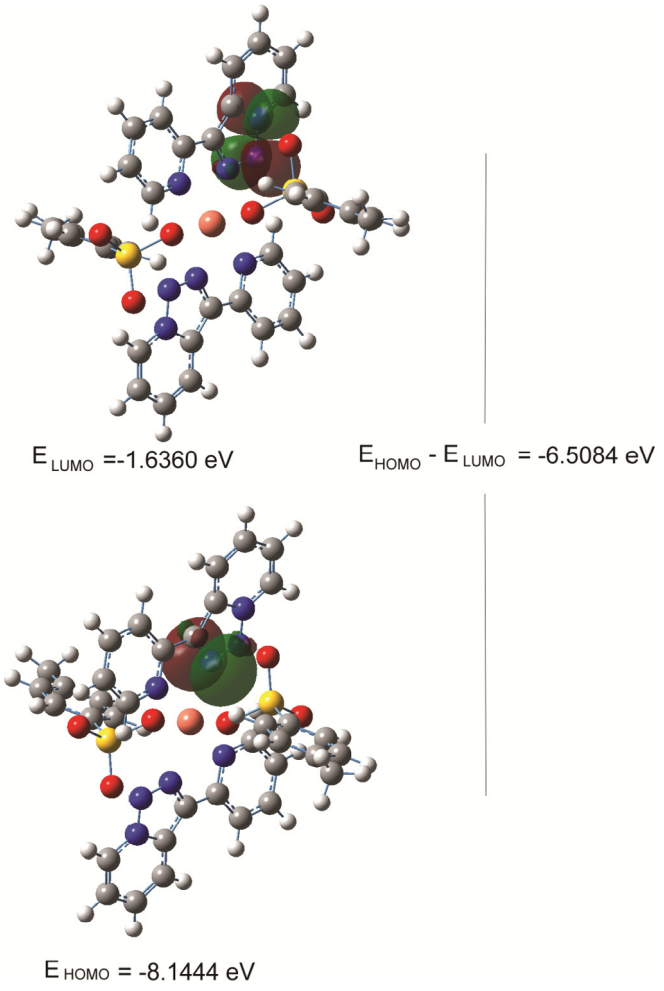

Fig. 9. The Homo and Lumo energy levels of the molecular structure by DFT/6–31G.

molecular orbital energy calculations that the molecule has a wide HOMO-LUMO range and consequently the structure exhibits stable and low chemical reactivity.

References

[1] W.R. Bamfordand, T.R. Stevens, J. Chem. Soc. 4735 (1952).
[2] R.H. Shapiro, Org. React. NY 23 (1975) 405.
[3] R.M. Adlingtonand, G.M. Barrett, Acc. Chem. Res. 16 (1983) 55.
[4] R.H. Shapiro, M.F. Lipton, K.J. Kolonko, R.L. Buswell, L.A. Capuano, Tetrahedron Lett. 16 (1975) 1811.
[5] V.K. Aggarwal, J.R. Fulton, C.G. Sheldon, J. de Vicente, J. Am. Chem. Soc. 125 (2003) 6034.
[6] V.K. Aggarwal, E. Alonso, G.Y. Fang, M. Ferrara, G. Hynd, M. Porcelloni, Angew. Chem. Int. Ed. 40 (2001) 1433.
[7] V.K. Aggarwal, J. de Vicente, R.V. Bonnert, J. Org. Chem. 68 (2003) 5381.
[8] Q. Xiao, Y. Xia, H. Li, Y. Zhang, J.B. Wang, Angew. Chem. Int. Ed. 50 (2011) 1114.
[9] L. Zhou, F. Ye, J.C. Ma, Y. Zhang, J.B. Wang, Angew. Chem. Int. Ed. 50 (2011) 3510.
[10] F. Ye, X.S. Ma, Q. Xiao, H. Li, Y. Zhang, J.B. Wang, J. Am. Chem. Soc. 134 (2012) 5742.
[11] G. Ye, Y. Shi, L. Zhou, Q. Xiao, Y. Zhang, J.B. Wang, Org. Lett. 13 (2011) 5020.
[12] L. Zhou, Y. Shi, Q. Xiao, Y.Z. Liu, F. Ye, Y. Zhang, J.B. Wang, Org. Lett. 13 (2011) 968.
[13] a) G. Jones, Adv. Heterocycl. Chem. 83 (2002) 1;
b) G. Jones, B. Abarca, Adv. Heterocycl. Chem. 100 (2010) 195.
[14] a) B. Abarca, R. Ballesteros, R. Ballesteros-Garrido, F. Colobert, F.R. Leroux, Tetrahedron 64 (2008) 3794;
b) B. Abarca, R. Ballesteros, F. Blanco, A. Bouillon, V. Collot, J.-R. Domı'nguez, J.-C. Lancelot, S. Rault, Tetrahedron 60 (20049 4887; c) B. Abarca, R. Ballesteros, M. Chadlaoui, Tetrahedron 60 (2004) 5785;
d) B. Abarca, R. Adam, R. Ballesteros, ARKIVOC (2010) 319;
e) B. Abarca, R. Adam, R. Ballesteros, L. Chiassai, C. Gamin, ARKIVOC (2012) 229;
f) B. Abarca, R. Ballesteros, M. Chadlaoui, J. Miralles, J.V. Murillo, D. Colonna, Tetrahedron 57 (2001) 10111;
g) B. Abarca-Gonzilez, J. Enzyme Inhib, Med. Chem. 17 (2002) 359.
[15] G. Maury, D. Meziane, D. Srairi, J.-P. Paugan, R. Paugam, Bull. Soc. Chim. Belg. 91 (1982) 153.
[16] a) B. Abarca, R. Ballesteros, M. Chadlaoui, C.R. de Arellano, J.A. Real, Eur. J. Inorg. Chem. 29 (2007) 4574;
b) K.A. Abboud, R.C. Palenik, G.J. Palenik, Inorg. Chim. Acta. 357 (2004) 321;
c) R. Ballesteros-Garrido, B. Abarca, R. Ballesteros, C.R. de Arellano, F.R. Leroux, F. Colobert, E. Garcia-EspaÇa, New J. Chem. 33 (2009) 2102;
d) M. Chadlaoui, B. Abarca, R. Ballesteros, C.R. de Arellano, J. Aguilar, R. Aucejo, E. Garcia-EspaÇa, J. Org. Chem. 71 (2006) 9030;
e) R. Ballesteros-Garrido, E. Delgado-Pinar, B. Abarca, R. Ballesteros, F.R. Leroux, F. Colobert, R.J. Zaragozi, E. Garcia-EspaÇa, Tetrahedron 68 (2012) 3701;
f) V. Niel, A.B. Gaspar, M.C. MuÇoz, B. Abarca, R. Ballesteros, J.A. Real, Inorg. Chem. 42 (2003) 4782;
g) J. Xiang, Y.G. Yin, P. Mei, Inorg. Chem. Commun. 10 (2007) 1168;
h) C.-F. Sheu, K. Chen, S.-M. Chen, Y.-S. Wen, G.-H. Lee, J.-M. Chen, J.-F. Lee, B.-M. Cheng, H.-S. Sheu, N. Yasuda, Y. Ozawa, K. Toriumi, Y. Wang, Chem. Eur J. 15 (2009) 2384;
i) O. Mamula, A. vonZelewsky, Coord. Chem. Rev. 242 (2003) 87;
j) C. Piguet, G. Bernardinelli, G. Hopfgartner, Chem. Rev. 97 (1997) 2005.
[17] L.P. Battaglia, M. Carcelli, F. Ferraro, L. Mavilla, C. Pelizzi, G. Pelizzi, J. Chem. Soc. Dalton Trans. 18 (1994) 2651.
[18] a) B. Abarca, I. Alkorta, R. Ballesteros, F. Blanco, M. Chadlaoui, J. Elguero, F. Mojarrad, Org. Biomol. Chem. 3 (2005) 3905;
b) J. Klingele, D. Kaase, J. Hilgert, G. Steinfeld, M.H. Klingele, J. Lach, Dalton Trans. 39 (2010) 4495;
c) E. Escriva, J. Server-Carrio, L. Lezama, J.V. Folgado, J.L. Pizarro, R. Ballesteros, B. Abarca, J. Chem. Soc. Dalton Trans. 12 (1997) 2033;
d) H.E. Zimmerman, A. Ignatchenko, J. Org. Chem. 64 (1999) 6635.
[19] a) O. Prakash, H.K. Gujral, N. Rani, S.P. Singh, Synth. Commun. 30 (2000) 417;
b) K. Wang, X. Fu, J. Liu, Y. Liang, D. Dong, Org. Lett. 11 (2009) 1015.
[20] J.H. Boyer, R. Borgers, L.T. Wolford, J. Am. Chem. Soc. 79 (19579 678.
[21] a) H. Ogura, S. Mineo, K. Nakagawa, S. Shiba, Yakugaku Zasshi 101 (1981) 329;
b) S. Mine, S. Kawamura, K. Nakagawa, Synth. Commun. 6 (1976) 69.
[22] A.D. Becke, J. Chem. Phys. 98 (1993) 5648.
[23] C. Lee, W. Yang, R.G. Parr, Phys. Rev. B37 (1988) 785.
[24] M.J. Frisch, G.W. Trucks, H.B. Schlegel, G.E. Scuseria, M.A. Robb, J.R. Cheeseman, G. Scalmani, V. Barone, B. Mennucci, G.A. Petersson, H. Nakatsuji, M. Caricato, X. Li, H.P. Hratchian, A.F. Izmaylov, J. Bloino, G. Zheng, J.L. Sonnenberg, M. Hada, M. Ehara, K. Toyota, R. Fukuda, J. Hasegawa, M. Ishida, T. Nakajima, Y. Honda, O. Kitao, H. Nakai, T. Vreven, J.A. Montgomery Jr., J.E. Peralta, F. Ogliaro, M. Bearpark, J.J. Heyd, E. Brothers, K.N. Kudin, V.N. Staroverov, R. Kobayashi, J. Normand, K. Raghavachari, A. Rendell, J.C. Burant, S.S. Iyengar, J. Tomasi, M. Cossi, N. Rega, J.M. Millam, M. Klene, J.E. Knox, J.B. Cross, V. Bakken, C. Adamo, J. Jaramillo, R. Gomperts, R.E. Stratmann, O. Yazyev, A.J. Austin, R. Cammi, C. Pomelli, J.W. Ochterski, R.L. Martin, K. Morokuma, V.G. Zakrzewski, G.A. Voth, P. Salvador, J.J. Dannenberg, S. Dapprich, A.D. Daniels, Ö. Farkas, J.B. Foresman, J.V. Ortiz, J. Cioslowski, D.J. Fox, Gaussian 09, Gaussian, Inc., Wallingford (CT, USA), 2009.
[25] G.M. Sheldrick, Acta Cryst. A71 (2015) 3.
[26] L.J. Farrugia, J. Appl. Crystallogr. 45 (2012) 849.
[27] G.M. Sheldrick, Acta Cryst C71 (2015) 3.
[28] V. Murugesan, M. Saravanabhavan, M. Sekar, J. Photochem. Photobiol. B Biol. 140 (2014) 20.
[29] C. Hongyan, T. Zhang, J. Zhang, Struct. Chem. 23 (2012) 153.
[30] T.M. Klapöke, J. Stierstorfer, B. Weber, Inorg. Chim. Acta. 362 (2009) 2311.
[31] B.K. Sharma, Spectroscopy (Goel, Meerut), 1999.
[32] Ç. Ağaç, İ. Yılmaz, A. Şengül, S. Coles, Turk. J. Chem. 34 (2010) 781.
[33] M. Petrova, R. Muhamadejev, B. Vigante, B. Cekavicus, A. Plotniece, G. Duburs, E. Liepinsh, Molecules 16 (2011) 8041.
[34] M.A. Spackman, P.G. Byrom, Chem. Phys. Lett. 267 (1997) 215.
[35] J.J. McKinnon, M.A. Spackman, A.S. Mitchell, Acta Cryst B60 (2004) 627.
[36] F.L. Hirshfeld, Their. Chim. Acta 44 (1977) 129.
[37] J.J. McKinnon, D. Jayatilaka, M.A. Spackman, Chem Commun (2007) 3814.
[38] M.J. Turner, J.J. McKinnon, S.K. Wolff, D.J. Grimwood, P.R. Spackman, D. Jayatilaka, M.A. Spackman, CrystalExplorer 17 (2017). University of Western Australia.
[39] P. Geerlings, F. De Proft, W. Langenaeker, Chem. Rev. 103 (5) (2003) 1793.
[40] R.G. Parr, L. Szentpaly, S. Liu, J. Am. Chem. Soc. 121 (9) (1999) 1922.
[41] J. Padmanabhan, R. Parthasarathi, V. Subramaniaan, P.K. Chattaraj, J. Phys. Chem. 111 (7) (2007) 1358.
[42] R.G. Parr, R.G. Pearson, J. Am. Chem. Soc. 105 (26) (1983) 7512.